Hindawi Publishing Corporation
Shock and Vibration
Volume 2014, Article ID 294163, 14 pages
http://dx.doi.org/10.1155/2014/294163

Research Article

Experimental Study of an Adaptive Sequential Nonlinear LSE with Unknown Inputs for Structural Damage Tracking

Tengfei Mu,[1] Li Zhou,[1] and Jann N. Yang[2]

[1] *State Key Laboratory of Mechanics and Control of Mechanical Structures, Nanjing University of Aeronautics and Astronautics, Nanjing 210016, China*
[2] *Department of Civil & Environmental Engineering, University of California, Irvine, CA 92697, USA*

Correspondence should be addressed to Li Zhou; lzhou@nuaa.edu.cn

Received 12 May 2013; Revised 9 January 2014; Accepted 25 February 2014; Published 16 March 2014

Academic Editor: Didier Rémond

An improved adaptive sequential nonlinear LSE with unknown inputs (ASNLSE-UI) approach was proposed to real-time-track the structural damage when it occurs for structural safety and management after emergency event. Experimental studies are presented to verify the capability of the improved ASNLSE-UI approach. A series of tests using a small-scale 3-story base-isolated building have been performed. White noise and earthquake excitations, applied to the base of the model, have been used. To simulate structural damages during the test, an innovative device is designed and manufactured to reduce the stiffness of some stories. With the measured response data of different damage scenarios, the improved ASNLSE-UI approach is used to track the variation of structural physical parameters. Besides, the unknown inputs are simultaneously identified. Experimental results demonstrate that the improved ASNLSE-UI approach is capable of tracking the variation of stiffness parameters leading to the detection of structural damages.

1. Introduction

One objective of the structural health monitoring system is to track the structural damage when it occurs for structural safety and management after emergency event [1, 2]. When a structural element is damaged, such as cracking or incompletion, generally the stiffness of the damaged element is reduced [3]. Hence, the structural damage can be reflected by the changes of parametric values of the damaged element. During a severe dynamic event, such as earthquake, and typhoon, a structure may be damaged, leading to the stiffness reductions of the damaged elements; thus the measured vibration data contains the information of damage events. In this regard, data analysis techniques for real-time damage tracking, based on vibration responses measured by sensors, have received considerable attention [4, 5].

Various approaches for structural parameter identification and damage tracking have been reported [6–13]. In these traditional approaches, all the external excitations should be measured by sensors. In practical applications, however, external inputs, such as seismic excitations and wind loads, may be not measured or even may be unmeasurable. Therefore, it is highly desirable to achieve parameter identification and damage tracking without using the excitation information [14, 15].

In the area of system identification with unknown inputs, some frequency domain approaches and time domain approaches have been developed. The frequency domain approaches, such as frequency domain decomposition [16] and mode decomposition [17], mainly concern structural modal parameters. The recognition accuracy of these approaches is high at steady state load but is negatively influenced at nonsteady state load. Furthermore, these approaches demand the reference data before damage as the baseline which may be unavailable or difficult to establish after a severe event and their ability of damage tracking is not strong during a severe event, such as a strong earthquake. The time domain approaches, such as stochastic subspace identification [18], random decrement technique [19], and parameter identification based on some hypothesis theories

[20, 21], mainly concern structural physical parameters. Due to the differences between the assumed and actual situations, additional errors are introduced undesirably in these time domain approaches. Although the two types of approaches are capable of identifying structural parameters, they cannot simultaneously identify system unknown inputs. These unknown inputs reflect the interaction between the structure and surrounding medium and are very significant to the research of surrounding medium, such as foundation soil mass and wind, flow. Consequently, it is important to develop real-time simultaneous identification of structural damage and load techniques based on incomplete measurements.

Several approaches for simultaneous identification of structural damage and load have been proposed, such as ILS-UI [22], statistical average [23], weighted average correction [24], and dynamic response sensitivity analysis [25]. However, some of these approaches can only identify constant structural parameters and load but cannot yield analytical solutions. Recently, analytical recursive solutions with adaptive damage tracking capabilities based on LSE-UI approach [26] and EKF-UI approach [27] have been derived to identify structural damage and load when the external excitations are not available. However, for practical applications of LSE-UI, only acceleration is measured, and velocity and displacement are usually obtained through numerical integrations of the acceleration data. Thus a significant numerical drift, difficult to be removed during the real-time data processing, may be introduced and magnified seriously when damage occurs. Besides, this approach only can deal with linear structures. In EKF-UI approach, due to the linearization of the state equation, the solution may not converge if the initial guesses of the parametric values are outside the region of convergence. In order to eliminate these drawbacks, a new technique, referred to as the adaptive sequential nonlinear least square estimation with unknown inputs (ASNLSE-UI) approach, has been proposed for real-time simultaneous identification of structural damage and load based on incomplete measurements [28]. Simulation results demonstrate that the ASNLSE-UI approach is capable of both tracking the variations of structural physical parameters, such as the degradation of stiffness due to structural damages, and identifying the unknown inputs [29]. Up to now, no experimental verifications have been made on the capability of the ASNLSE-UI approach to track structural damage, especially for the nonlinear hysteretic system [30].

In this research, experimental studies are performed and presented to verify the capability of the ASNLSE-UI approach in identifying the structural damage and load simultaneously. A series of tests using a scaled 3-story base-isolated building model widely used to withstand earthquakes has been performed. The Bouc-Wen model [31] is used to represent the inelastic behavior of rubber-bearing isolators. Furthermore, a species-based quantum-behaved particle swarm optimization (SQPSO) algorithm [32] is used to improve the adaptive capability of the approach for damage tracking. Different types of excitations applied at the base of the building model have been used, including the white noise excitations, El Centro earthquake excitation, and Kobe earthquake excitation. To simulate structural damages during the test, an innovative device based on the concept of structural control is proposed to reduce the stiffness of some stories, referred to as the stiffness element device (SED) [33]. Different damage scenarios have been simulated and tested. With the measured acceleration response data, the improved ASNLSE-UI approach is used to track the variation of story stiffness and identify the unknown inputs from the base during the test. The tracking results of story stiffness are used to be compared with the ones computed based on the finite element method (FEM), and the identified unknown inputs are also used to be compared with the ones measured in the tests. The comparisons show that the ASNLSE-UI approach is capable of real-time tracking the damages of base-isolated building and identifying the unknown inputs simultaneously.

2. Adaptive Sequential Nonlinear LSE with Unknown Inputs (ASNLSE-UI)

The equation of motion of a m-DOF nonlinear structure can be expressed as

$$\mathbf{M}\ddot{\mathbf{x}}(t) + \mathbf{F}_c[\dot{\mathbf{x}}(t), \boldsymbol{\theta}] + \mathbf{F}_s[\mathbf{x}(t), \boldsymbol{\theta}] = \boldsymbol{\eta}\mathbf{f}(t) + \boldsymbol{\eta}^*\mathbf{f}^*(t) \quad (1)$$

in which, $\mathbf{x}(t)$, $\dot{\mathbf{x}}(t)$, and $\ddot{\mathbf{x}}(t)$ are the displacement vector, velocity vector, and acceleration vector, respectively. $\mathbf{M}$ is the mass matrix. $\mathbf{F}_c[\dot{\mathbf{x}}(t), \boldsymbol{\theta}]$ is the damping force vector. $\mathbf{F}_s[\mathbf{x}(t), \boldsymbol{\theta}]$ is the stiffness force vector. $\mathbf{f}(t)$ and $\mathbf{f}^*(t)$ are the known and unknown excitations (system inputs), which are the influence matrixes $\boldsymbol{\eta}$ and $\boldsymbol{\eta}^*$ corresponding to. $\boldsymbol{\theta} = [\theta_1, \theta_2, \ldots, \theta_n]^{\mathrm{T}}$ is the unknown parametric vector of the structure, involving n unknown parameters θ_i $(i = 1, 2, \ldots, n)$, such as stiffness, damping, and nonlinear hysteretic parameters, which may be time-varying and need to be tracked.

For simplicity consideration, assume that the unknown parametric vector $\boldsymbol{\theta}$ is constant, that is, $\boldsymbol{\theta} = \boldsymbol{\theta}_1 = \boldsymbol{\theta}_2 = \cdots = \boldsymbol{\theta}_{k+1}$, where $\boldsymbol{\theta}_i = \boldsymbol{\theta}(t = i\Delta t)$ for $i = 1, 2, \ldots, k+1$, and that the mass matrix $\mathbf{M}$ is known and constant. The masses can be considered as unknown, in which cases the unknown masses will be included in the parametric vector $\boldsymbol{\theta}_i$. Likewise, $\boldsymbol{\eta}^*$ is a null matrix if all excitations are measured, and $\boldsymbol{\eta}$ is a null matrix if all excitations are not measured. For present investigations, the unknown quantities to be identified are the unknown parametric vector $\boldsymbol{\theta}$, the unmeasured excitation vector $\mathbf{f}^*(t)$, and the state vector $\mathbf{X} = [\mathbf{x}^{\mathrm{T}}, \dot{\mathbf{x}}^{\mathrm{T}}]^{\mathrm{T}}$, including the displacement and velocity vectors. In what follows, the bold face letter represents either a vector or a matrix.

The observation equation can be obtained from (1) as follows:

$$\boldsymbol{\varphi}(\mathbf{X})\boldsymbol{\theta} + \boldsymbol{\varepsilon} = \overline{\boldsymbol{\eta}}\overline{\mathbf{f}} + \mathbf{y}, \quad (2)$$

where $\boldsymbol{\varphi}(\mathbf{X})$ is data matrix, $\overline{\mathbf{f}} = \mathbf{f}^*$ is an unknown input vector, $\overline{\boldsymbol{\eta}} = \boldsymbol{\eta}^*$ is the influence matrix of $\overline{\mathbf{f}}$, $\mathbf{y} = \boldsymbol{\eta}\mathbf{f} - \mathbf{M}\ddot{\mathbf{x}}(t)$ is known, and ε is a model noise vector, respectively.

In the ASNLSE-UI approach, an extended unknown vector $\boldsymbol{\theta}_{e,k}$ at $t_k(t_k = k\Delta t)$ is introduced; namely, $\boldsymbol{\theta}_{e,k} = [\boldsymbol{\theta}_k, \overline{\mathbf{f}}_k]^{\mathrm{T}}$; thus (2) can be discretized as

$$\boldsymbol{\varphi}_{e,k}(\mathbf{X}_k)\boldsymbol{\theta}_{e,k} + \boldsymbol{\varepsilon}_k = \mathbf{y}_k. \quad (3)$$

$\mathbf{X}_k$ and $\boldsymbol{\theta}_{e,k}$ can be solved in two steps as follows [28].

Step I. Suppose that the state vector $\mathbf{X}_k$ is known. Based on (2) and (3), the general objective function, namely, the sum of the square error between the known vector $\mathbf{y}$ and the identified vector $\boldsymbol{\varphi}(\mathbf{X})\boldsymbol{\theta}$, can be expressed by

$$\mathbf{J}_{k+1}\left(\boldsymbol{\theta}_{e,k}\right) = \sum_{i=1}^{k+1}\left[\mathbf{y}_i - \boldsymbol{\varphi}_{e,i}\left(\mathbf{X}_i\right)\boldsymbol{\theta}_{e,i}\right]^{\mathrm{T}}\left[\mathbf{y}_i - \boldsymbol{\varphi}_{e,i}\left(\mathbf{X}_i\right)\boldsymbol{\theta}_{e,i}\right]. \quad (4)$$

If the number of DOFs of the structure is greater than the total number of unknown inputs and the rank of $\boldsymbol{\varphi}(\mathbf{X})$ is full, the LSE approach can be used to minimize the objective function given by (4) to yield the recursive LSE solution for the extended unknown vector $\boldsymbol{\theta}_{e,k+1}$. Then the recursive solutions for $\widehat{\boldsymbol{\theta}}_{k+1}$ and $\widehat{\bar{\mathbf{f}}}_{k+1|k+1}$ (the estimates of $\boldsymbol{\theta}_{k+1}$ and $\bar{\mathbf{f}}_{k+1}$) are determined as follows:

$$\widehat{\boldsymbol{\theta}}_{k+1} = \widehat{\boldsymbol{\theta}}_k + \mathbf{K}_{\boldsymbol{\theta},k+1}\left(\mathbf{X}_{k+1}\right)\left[\mathbf{y}_{k+1} - \boldsymbol{\varphi}_{k+1}\left(\mathbf{X}_{k+1}\right)\widehat{\boldsymbol{\theta}}_k + \overline{\boldsymbol{\eta}}\widehat{\bar{\mathbf{f}}}_{k+1|k+1}\right], \quad (5)$$

$$\widehat{\bar{\mathbf{f}}}_{k+1|k+1} = -\mathbf{S}_{k+1}\left(\mathbf{X}_{k+1}\right)\overline{\boldsymbol{\eta}}^{\mathrm{T}}\left[\mathbf{I} - \boldsymbol{\varphi}_{k+1}\left(\mathbf{X}_{k+1}\right)\mathbf{K}_{\boldsymbol{\theta},k+1}\left(\mathbf{X}_{k+1}\right)\right] \times \left[\mathbf{y}_{k+1} - \boldsymbol{\varphi}_{k+1}\left(\mathbf{X}_{k+1}\right)\widehat{\boldsymbol{\theta}}_k\right], \quad (6)$$

$$\mathbf{K}_{\boldsymbol{\theta},k+1}\left(\mathbf{X}_{k+1}\right) = \left(\boldsymbol{\Lambda}_{k+1}\mathbf{P}_{\boldsymbol{\theta},k}\boldsymbol{\Lambda}_{k+1}^{\mathrm{T}}\right)\boldsymbol{\varphi}_{k+1}^{\mathrm{T}}\left(\mathbf{X}_{k+1}\right) \times \left[\mathbf{I} + \boldsymbol{\varphi}_{k+1}\left(\mathbf{X}_{k+1}\right)\left(\boldsymbol{\Lambda}_{k+1}\mathbf{P}_{\boldsymbol{\theta},k}\boldsymbol{\Lambda}_{k+1}^{\mathrm{T}}\right) \times \boldsymbol{\varphi}_{k+1}^{\mathrm{T}}\left(\mathbf{X}_{k+1}\right)\right]^{-1}, \quad (7)$$

$$\mathbf{S}_{k+1}\left(\mathbf{X}_{k+1}\right) = \left\{\overline{\boldsymbol{\eta}}^{\mathrm{T}}\left[\mathbf{I} - \boldsymbol{\varphi}_{k+1}\left(\mathbf{X}_{k+1}\right)\mathbf{K}_{\boldsymbol{\theta},k+1}\left(\mathbf{X}_{k+1}\right)\right]\overline{\boldsymbol{\eta}}\right\}^{-1}, \quad (8)$$

$$\mathbf{P}_{\boldsymbol{\theta},k+1} = \left[\mathbf{I} + \mathbf{K}_{\boldsymbol{\theta},k+1}\left(\mathbf{X}_{k+1}\right)\overline{\boldsymbol{\eta}}\mathbf{S}_{k+1}\left(\mathbf{X}_{k+1}\right)\overline{\boldsymbol{\eta}}^{\mathrm{T}}\boldsymbol{\varphi}_{k+1}\left(\mathbf{X}_{k+1}\right)\right] \times \left(\mathbf{I} - \mathbf{K}_{\boldsymbol{\theta},k+1}\left(\mathbf{X}_{k+1}\right)\boldsymbol{\varphi}_{k+1}\left(\mathbf{X}_{k+1}\right)\right)\left(\boldsymbol{\Lambda}_{k+1}\mathbf{P}_{\boldsymbol{\theta},k}\boldsymbol{\Lambda}_{k+1}^{\mathrm{T}}\right) \quad (9)$$

in which, $\mathbf{K}_{\boldsymbol{\theta},k+1}(\mathbf{X}_{k+1})$ is the LSE gain matrix for $\widehat{\boldsymbol{\theta}}_{k+1}$, $\boldsymbol{\varphi}_{k+1}(\mathbf{X}_{k+1})$ is the observation matrix composed of the system response vectors, and $\mathbf{P}_{\boldsymbol{\theta},k+1}$ is the adaptation gain matrix [26].

Step II. Since $\boldsymbol{\theta}_{k+1}$ and $\mathbf{X}_{k+1}$ are interrelated, the estimate $\widehat{\boldsymbol{\theta}}_{k+1}$ is a function of the unknown state vector b_{k+1}; that is, $\widehat{\boldsymbol{\theta}}_{k+1} = \widehat{\boldsymbol{\theta}}_{k+1}(\mathbf{X}_{k+1})$. It follows from (4) that the general objective function should be expressed as

$$\mathbf{J}_{k+1}\left(\mathbf{X}_{k+1}\right) = \sum_{i=1}^{k+1}\left[\mathbf{y}_i - \boldsymbol{\varphi}_i\left(\mathbf{X}_i\right)\widehat{\boldsymbol{\theta}}_i\left(\mathbf{X}_i\right) + \overline{\boldsymbol{\eta}}\bar{\mathbf{f}}_i\right]^{\mathrm{T}} \times \left[\mathbf{y}_i - \boldsymbol{\varphi}_i\left(\mathbf{X}_i\right)\widehat{\boldsymbol{\theta}}_i\left(\mathbf{X}_i\right) + \overline{\boldsymbol{\eta}}\bar{\mathbf{f}}\right]. \quad (10)$$

And the unknown state vector $\mathbf{X}_{k+1}$ will be estimated by further minimizing the general objective function of (10). Since (10) is highly nonlinear in unknown state vector $\mathbf{X}_{k+1}$, the recursive solutions for $\widehat{\mathbf{X}}_{k+1|k+1}$ (the estimate of $\mathbf{X}_{k+1}$) are derived as follows:

$$\widehat{\mathbf{X}}_{k+1|k+1} = \widehat{\mathbf{X}}_{k+1|k} + \overline{\mathbf{K}}_{k+1}\left[\mathbf{y}_{k+1} - \widehat{\mathbf{y}}_{k+1}\left(\widehat{\mathbf{X}}_{k+1|k}\right)\right] \quad (11)$$

in which $\widehat{\mathbf{y}}_{k+1}[\mathbf{X}_{k+1}(\mathbf{X}_k)] = \boldsymbol{\varphi}_{k+1}[\mathbf{X}_{k+1}(\mathbf{X}_k)]\widehat{\boldsymbol{\theta}}_{k+1}[\mathbf{X}_{k+1}(\mathbf{X}_k)] - \overline{\boldsymbol{\eta}}\widehat{\bar{\mathbf{f}}}_{k+1}$, and

$$\widehat{\mathbf{X}}_{k+1|k} = \boldsymbol{\Phi}_{k+1,k}\widehat{\mathbf{X}}_{k|k} + \mathbf{B}_1\ddot{\mathbf{x}}_k + \mathbf{B}_2\ddot{\mathbf{x}}_{k+1}, \quad (12)$$

$$\overline{\mathbf{K}}_{k+1} = \overline{\mathbf{P}}_{k+1|k}\boldsymbol{\Psi}^{\mathrm{T}}{}_{k+1,k+1}\left[\mathbf{I} + \boldsymbol{\Psi}_{k+1,k+1}\overline{\mathbf{P}}_{k+1|k}\boldsymbol{\Psi}^{\mathrm{T}}{}_{k+1,k+1}\right]^{-1} \quad (13)$$

$$\overline{\mathbf{P}}_{k+1|k} = \boldsymbol{\Phi}_{k+1,k}\overline{\mathbf{P}}_{k|k}\boldsymbol{\Phi}_{k+1,k}^{\mathrm{T}}, \quad (14)$$

$$\overline{\mathbf{P}}_{k|k} = \left(\mathbf{I} - \overline{\mathbf{K}}_k\boldsymbol{\Psi}_{k,k}\right)\overline{\mathbf{P}}_{k+1|k}, \quad (15)$$

where

$$\boldsymbol{\Phi}_{k+1,k}\begin{Bmatrix}\mathbf{I} & \Delta\mathbf{t}\mathbf{I}\\ \mathbf{0} & \mathbf{I}\end{Bmatrix},$$

$$\boldsymbol{\Psi}_{i,k+1} = \left[\frac{\partial\widehat{\mathbf{y}}_i\left(\mathbf{X}_i\right)}{\partial\mathbf{X}_i}\cdot\frac{\partial\mathbf{X}_i}{\partial\mathbf{X}_{k+1}}\right]_{\mathbf{X}_i=\mathbf{X}_i\left(\widehat{\mathbf{X}}_{k+1|k}\right),}, \quad (16)$$

$$\mathbf{B}_1 = \begin{bmatrix}\left(0.5-\beta\right)\left(\Delta\mathbf{t}\right)^2\mathbf{I}\\ \left(1-\gamma\right)\left(\Delta\mathbf{t}\right)\mathbf{I}\end{bmatrix}, \qquad \mathbf{B}_2 = \begin{bmatrix}\beta\left(\Delta\mathbf{t}\right)^2\mathbf{I}\\ \gamma\left(\Delta\mathbf{t}\right)\mathbf{I}\end{bmatrix}.$$

In (16), β and γ are parameters used in the Newmark-β method (usually $\beta = 0.25$, $\gamma = 0.5$), and $\mathbf{I}$ represents a unit matrix. As is shown, $\widehat{\boldsymbol{\theta}}_{k+1}$, $\widehat{\bar{\mathbf{f}}}_{k+1|k+1}$ and $\widehat{\mathbf{X}}_{k+1|k+1}$ are interrelated with one another, usually $\widehat{\mathbf{X}}_{k+1|k+1}$ is acceptable if $\widehat{\boldsymbol{\theta}}_{k+1}$ and $\widehat{\bar{\mathbf{f}}}_{k+1|k+1}$ are accurate. Consequently, only the identified results of $\widehat{\boldsymbol{\theta}}_{k+1}$ and $\widehat{\bar{\mathbf{f}}}_{k+1|k+1}$ are presented for comparisons.

In (7) and (9), based on the adaptive tracking technique proposed in [28], the adaptive factor matrix $\boldsymbol{\Lambda}_{k+1}$ can be implemented to identify time-varying parameters of the structures for detecting the damages. In [28], the optimal solution for the adaptive factor matrix $\boldsymbol{\Lambda}_{k+1}$ is searched by the function "CONSTR" or "fmincon" in MATLAB based on the constrained optimization. Since this function may cause the complex solution leading to the failure in program process or the divergence of the identified result, therefore, based on the constrained optimization, a process of solving $\boldsymbol{\Lambda}_{k+1}$ is attempted by using genetic algorithm to overcome the drawbacks. Unfortunately, the method is likely to converge to a local optimum, besides, its convergence speed is low [34]. To improve the convergence characteristics, a species-based quantum-behaved particle swarm optimization (SQPSO)

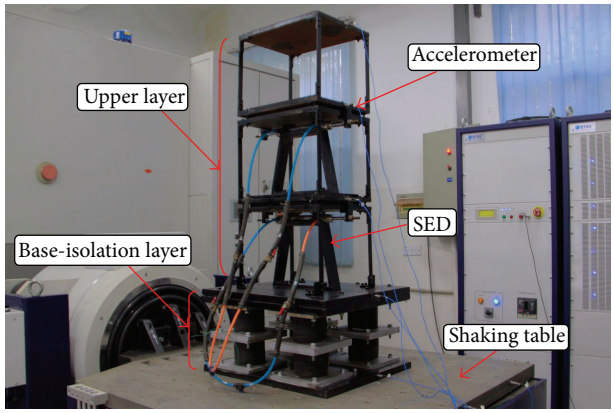

Figure 1: Test base-isolated building model on shake table.

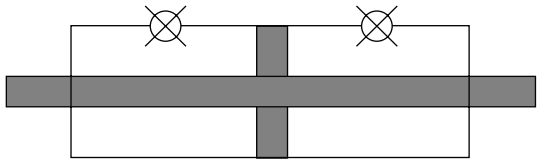

Figure 2: Schematic diagram of hydraulic cylinder-piston system.

algorithm [32] is used for the process of solving $\boldsymbol{\Lambda}_{k+1}$ based on the constrained optimization. Details are given as follows:

$$\begin{aligned} \min \quad & f\left[\widehat{\boldsymbol{\theta}}_{k+1}\left(\boldsymbol{\Lambda}_{k+1}\right)\right] = \sum_{j=1}^{n}\left|\frac{\widehat{\theta}_j(k+1)-\widehat{\theta}_j(k)}{\widehat{\theta}_j(k)}\right| \\ \text{s.t.} \quad & \left\|\mathbf{V}_{k+1}-\left[\mathbf{I}+\boldsymbol{\varphi}_{k+1}\left(\boldsymbol{\Lambda}_{k+1}\mathbf{P}_{\boldsymbol{\theta},k}\boldsymbol{\Lambda}_{k+1}^{\mathrm{T}}\right)\boldsymbol{\varphi}_{k+1}^{\mathrm{T}}\right]\right. \\ & \left.\times\,\boldsymbol{\sigma}_{k+1}^{2}\left[\mathbf{I}+\boldsymbol{\varphi}_{k+1}\left(\boldsymbol{\Lambda}_{k+1}\mathbf{P}_{\boldsymbol{\theta},k}\boldsymbol{\Lambda}_{k+1}^{\mathrm{T}}\right)\boldsymbol{\varphi}_{k+1}^{\mathrm{T}}\right]^{\mathrm{T}}\right\| \\ & \le \delta \end{aligned} \tag{17}$$

in which $\|\cdot\|$ is the norm of a matrix, δ is a small positive constant (e.g., $\delta = 10^{-2}$), and $\boldsymbol{\sigma}_{k+1}^2$ is the model noises that could be estimated through the signal information. This approach is referred to as the improved adaptive sequential nonlinear least square estimation with unknown inputs (ASNLSE-UI). To initiate the recursive solution, the initial values for the unknown parametric vector $\boldsymbol{\theta}$, the unmeasured excitation vector $\mathbf{f}^*(t)$, and the unknown state vector $\mathbf{X} = [\mathbf{x}^{\mathrm{T}}, \dot{\mathbf{x}}^{\mathrm{T}}]^{\mathrm{T}}$ should be assumed. Likewise, the initial gain matrixes $\mathbf{P}_0$ for the parametric vector and $\mathbf{P}_{0|0}$ for the state vector should be assigned.

3. Experimental Studies

3.1. Experimental Setup. The small-scale base-isolated building model, which consists of a base-isolation layer and a three-story building, as shown in Figure 1, is used for the experiment. The 400 mm by 300 mm building mounted on the 600 mm by 500 mm base-isolation layer, made up of 8 circular rubber-bearings (GZN110) with a diameter of 110 mm. The total height of this model is 1350 mm, with the height of upper layer being 1035 mm (each story being identical to 345 mm) and the height of the base-isolation layer being 315 mm. The total weight of the model is 383 kg, including the mass of the base-isolation layer being $m_1 = 255.5$ kg and the mass of upper layer being 127.5 kg with the mass distributing of each story as $m_2 = 54.5$ kg, $m_3 = 48.5$ kg, and $m_4 = 24.5$ kg. The first four natural frequencies of the test specimen are 1.650 Hz, 3.356 Hz, 6.941 Hz, and 10.024 Hz. Based on the experimental data and the discretized shear-beam model using the finite element method (FEM), the stiffness of each story is obtained as $k_1 = 50.9$ kN/m, $k_2 = 45.9$ kN/m, $k_3 = 46.1$ kN/m, and $k_4 = 55.4$ kN/m, respectively, referred to as the reference values of identified stiffness.

Two types of external excitations will be used, including the white noise excitation with different amplitudes and earthquake excitations including El Centro earthquake excitation and Kobe earthquake excitation. For all the external excitations, the base-isolated building model is placed on the shaking table (ETS GT1200 M) which is used to simulate different kinds of base excitations by the vibration controller (UCON VT-9008). During the tests, each story is installed with one acceleration sensor (PCB 3701G3FA3G) to measure the vibration responses by data acquisition system (NI PXI 4472B). The sampling frequency is 1000 Hz for all measurements.

3.2. Stiffness Element Device (SED). The damage in a story unit is assumed to be reflected by the reduction of its stiffness. To simulate the reductions of the stiffness in a selected story unit, say ith story, a stiffness element device (SED) with an effective stiffness of K_{hi} will be installed in the ith story unit, so that the stiffness of the ith story unit is increased by K_{hi}. During the experimental test, the effective stiffness of the SED is reduced to zero to simulate the reduction of the stiffness in the ith story unit due to damages. The innovative concept for the SED is motivated by the so-called resettable semiactive stiffness dampers [35].

Consider a device consisting of a hydraulic cylinder-piston (HCP) system with one valve on each side of the piston as shown in Figure 2. With both valves being closed, the cylinder is filled with pressurized gas. Hence, the HCP serves as a stiffness element in which the stiffness is provided by the bulk modulus of the pressurized gas in the cylinder. When both valves are open, the piston is free to move and the stiffness of the HCP becomes zero. For simulating the stiffness reduction in a selected story unit, the HCP is connected to a bracing system and installed in the selected story unit as shown in Figure 3(a). In Figure 3(a), the HCP is fixed to the bracing system in the second and third story, and the piston is connected to the second and third floor. Hence, the HCP and the bracing system are connected in series. The entire system, consisting of the HCP and the bracing system, is referred to as the stiffness element device.

Suppose the stiffness of the HCP is denoted by K_{ei} and that of the bracing system in the ith story is denoted by K_{bi}.

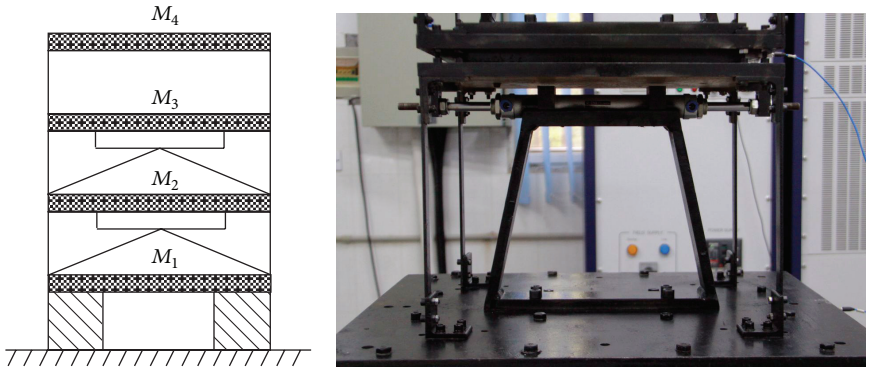

FIGURE 3: A base-isolated building model equipped with two stiffness element devices in the second and third stories: (a) schematic figure and (b) actual installation in the second story.

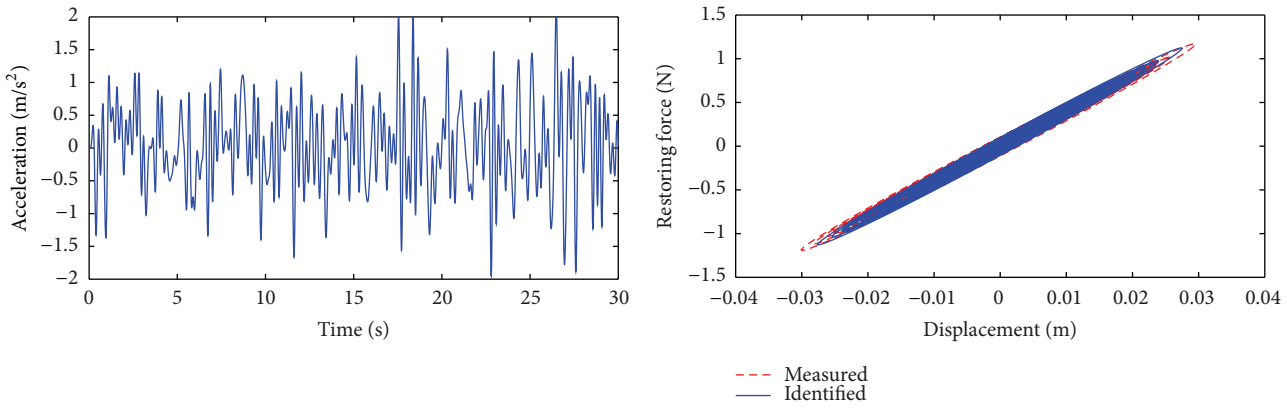

FIGURE 4: Test results for preexperiment: (a) white noise excitation; (b) hysteresis loops.

Then, the effective stiffness of the entire SED, denoted by K_{hi}, is given by

$$K_{hi} = \frac{K_{ei}K_{bi}}{(K_{ei} + K_{bi})}. \tag{18}$$

In this experimental setup, the stiffness of the bracing system K_{bi} is much bigger than that of the HCP; that is, $K_{bi} \gg K_{ei}$ (K_{bi} is about three orders of magnitude bigger than K_{ei}). Hence, the effective stiffness of the entire SED, consisting of the HCP and the bracing system, is approximately equal to that of the HCP; that is, $K_{hi} = K_{ei}$. With the installation of the SED in the second or third story as shown in Figure 3(a), the stiffness of the second or third story is increased by K_{hi}.

The stiffness of the HCP, K_{ei}, depends on the magnitude of the gas pressure in the cylinder. It has been demonstrated that K_{ei} is linearly proportional to the gas pressure P_0 [33]; that is,

$$K_{ei} = GP_0, \tag{19}$$

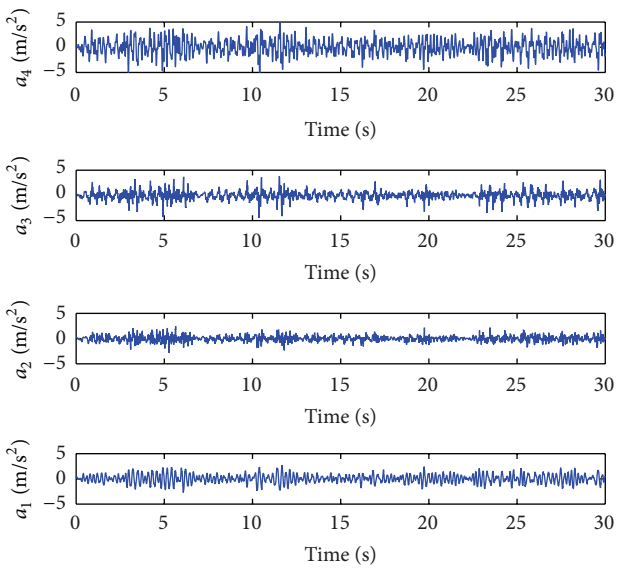

FIGURE 5: Measured acceleration responses for Case 1.

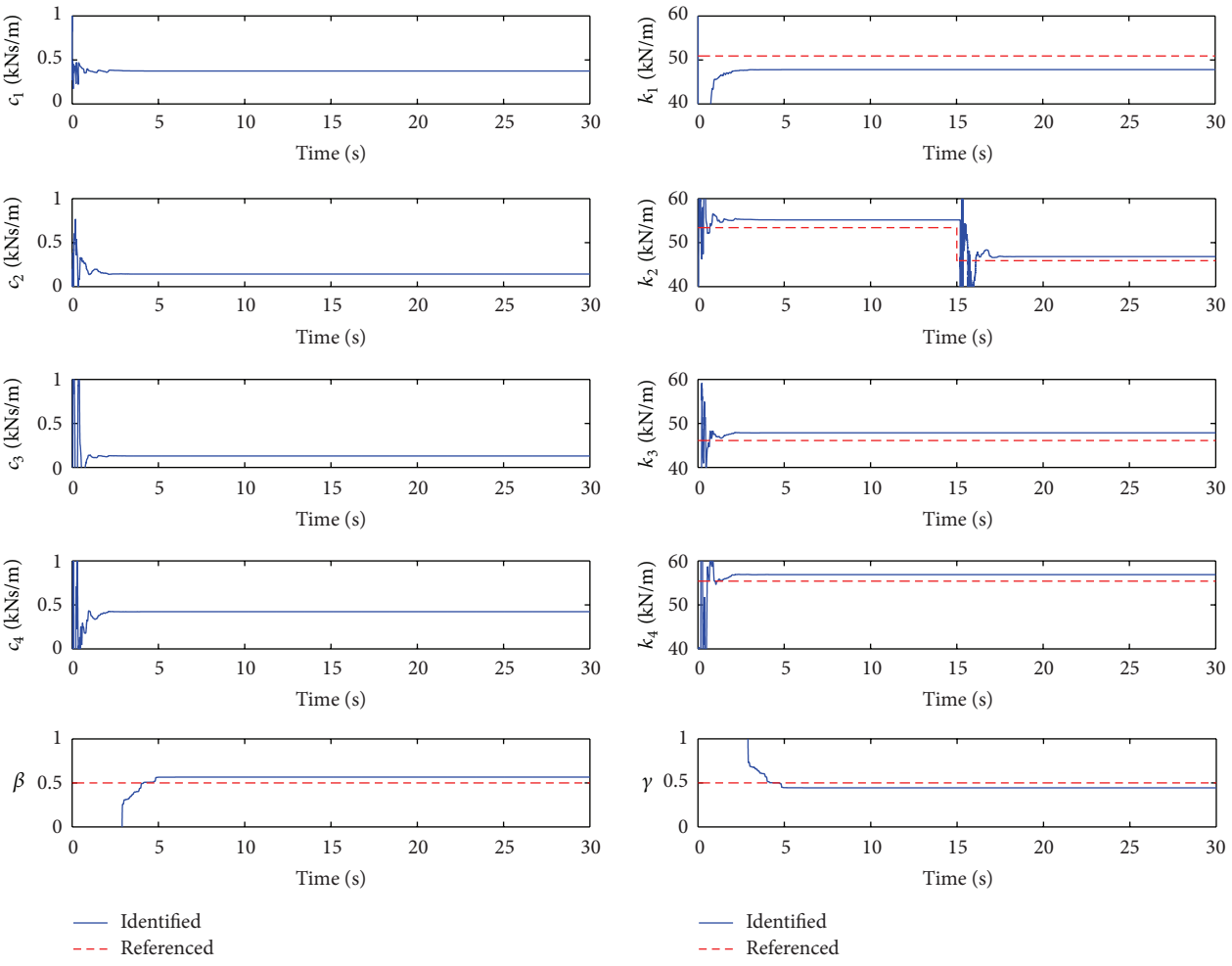

(a)

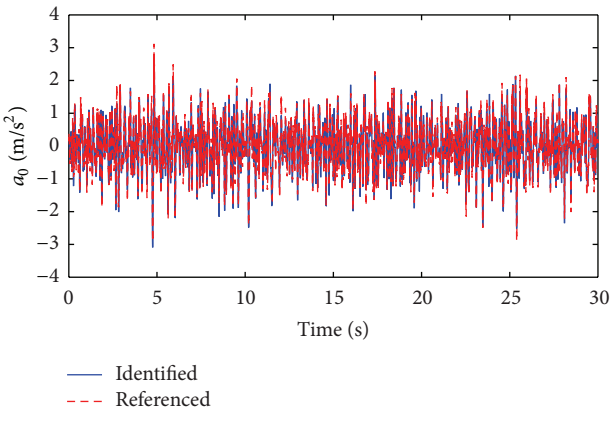

(b)

Figure 6: Identified results for Case 1: (a) identified parameters and (b) identified excitation.

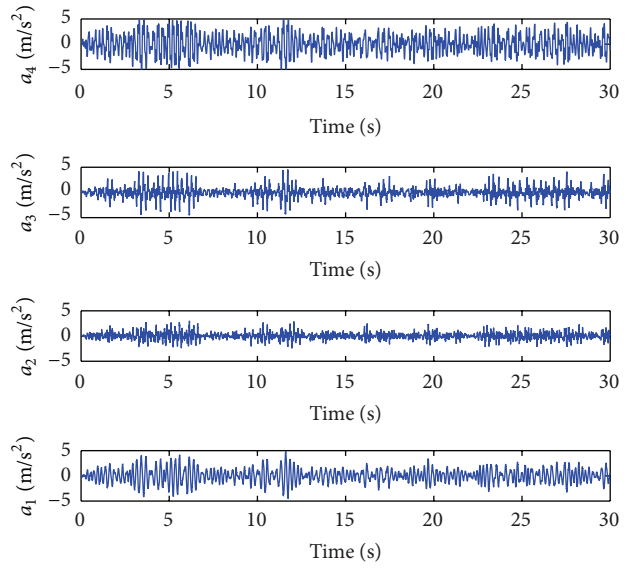

FIGURE 7: Measured acceleration responses for Case 2.

where G is a constant depending on the dimension of the cylinder and the property of the fluid or gas. Consequently, the desirable effective stiffness, K_{hi}, of the SED can be achieved by adjusting the gas pressure P_0 in the cylinder.

To simulate the reduction of stiffness in the ith story, a SED system is installed in the ith story, so that the stiffness of the ith story is increased by $K_{hi} = K_{ei}$. During the test, two valves of the SED are open simultaneously at the time instant, t_r, so that K_{hi} becomes zero, thus reducing the stiffness of the ith story by an amount of K_{ei} at $t = t_r$. Based on (19), the selection of the gas pressure, P_0, depends on the magnitude of the stiffness, K_{hi}, to be reduced in the ith story unit. The installation of a SED system in the second story of the test specimen is shown in Figure 3(b).

3.3. Analytical Model for Base-Isolated Building. To identify the parameters and loads of base-isolated building model using the ASNLSE-UI approach, a suitable analytical model should be built, especially for the rubber-bearing isolators. Several hysteretic models for describing the dynamic behavior of rubber-bearings have been proposed in [31, 36–38]. The determination of a proper model for the rubber-bearing is usually based on the deformation-restoring force characteristic obtained from static or dynamic experiments. However, the determination of an appropriate model for the base isolation system using actual response data is important in civil engineering applications. To date, no single model has proven satisfactory for all hysteretic systems for one reason or another. For rubber-bearing isolators, the Bouc-Wen model seems to be quite reasonable to delineate the dynamic characteristics of the nonlinear hysteretic vibration isolation system [31, 36]. Some static and dynamic testing results of this base-isolation layer used in this research can be found elsewhere [39, 40]. The motion equation of the base-isolated structure can be expressed as

$$\begin{aligned} m_1\left(\ddot{x}_1 + \ddot{x}_0\right) &= -r_1 + r_2, \\ m_2\left(\ddot{x}_2 + \ddot{x}_0\right) &= -r_2 + r_3, \\ m_3\left(\ddot{x}_3 + \ddot{x}_0\right) &= -r_3 + r_4, \\ m_4\left(\ddot{x}_4 + \ddot{x}_0\right) &= -r_4, \\ \dot{r}_1 &= c_1\ddot{x}_1 + k_1\dot{x}_1 - \beta\left|\dot{x}_1\right|\left|r_1\right|^{n-1}r_1 - \gamma\dot{x}_1\left|r_1\right|^n, \\ \dot{r}_i &= c_i\left(\ddot{x}_i - \ddot{x}_{i-1}\right) + k_i\left(\dot{x}_i - \dot{x}_{i-1}\right), \quad i = 2, 3, 4 \end{aligned} \tag{20}$$

in which, x is the relative displacement, $r_1 = r_1(x_1, \dot{x}_1)$ is the nonlinear hysteretic restoring force, and r_i $(i = 2, 3, 4)$ contains damping force and stiffness force. The Boun-Wen model is used for $r_1 = r_1(x_1, \dot{x}_1)$ as $\dot{r}_1 = \dot{r}_1(x_1, \dot{x}_1)$, in which β, γ, and n are hysteretic parameters that β and γ are basic hysteresis shape control and n is sharpness of yielding. According to the experimental results, hysteretic parameter n is considered to be 2 for the smooth hysteresis loops, so $n = 2$ is adopted to reduce computational efforts [40]. For rubber-bearings $\beta + \gamma = 1$ has been demonstrated. Furthermore, $\beta = 0.5$ and $\gamma = 0.5$ are obtained based on the experimental data as the reference values of the hysteretic parameters in this research. Consequently, the unknown parametric vector is $\boldsymbol{\theta} = [c_1, c_2, c_3, c_4, k_1, k_2, k_3, k_4, \beta, \gamma]$ and the unmeasured excitation is $\ddot{x}_0$. The measured vector in (3) is defined as $\mathbf{y}_k = [y_{1,k}, y_{2,k}, y_{3,k}, y_{4,k}]$, and $y_{i,k}$ obtained from the measured data can be expressed as [26]

$$y_{i,k} = \left(\frac{12}{\Delta t}\right)\left(r_{1,k} - r_{2,k-1}\right). \tag{21}$$

Also, based on a third-order corrector method [41], $\widehat{y}_{i,k}$ can be expressed through the estimated data as follows:

$$\widehat{y}_{i,k} = 5\dot{r}_{i,k} + 8\dot{r}_{i,k-1} - \dot{r}_{i,k-2}. \tag{22}$$

The data matrix $\boldsymbol{\varphi}_k$ can be easily obtained by using (20) and (22). Then (3) can be constructed. Finally, based on the accelerator responses, analytical model for base-isolated building, and ASNLSE-UI approach, the damage tracking and the unknown load identification can be carried out effectively.

4. Results and Discussions

To demonstrate the capability of the ASNLSE-UI approach for parametric and load identifications and real-time damage tracking of base-isolated structures, a scaled 3-story base-isolated building model subject to different types of excitations, applied to the base of the model driven by shake table with different damage scenarios of the structures, is considered experimentally. A band-limited white noise excitation in the frequency range of 1–20 Hz with a peak ground acceleration (PGA) of 0.22 g, shown in Figure 4(a), is used to drive the shake table as a preexperiment for ensuring that the nonlinear behavior of the base-isolated building actually takes place even under the circumstance

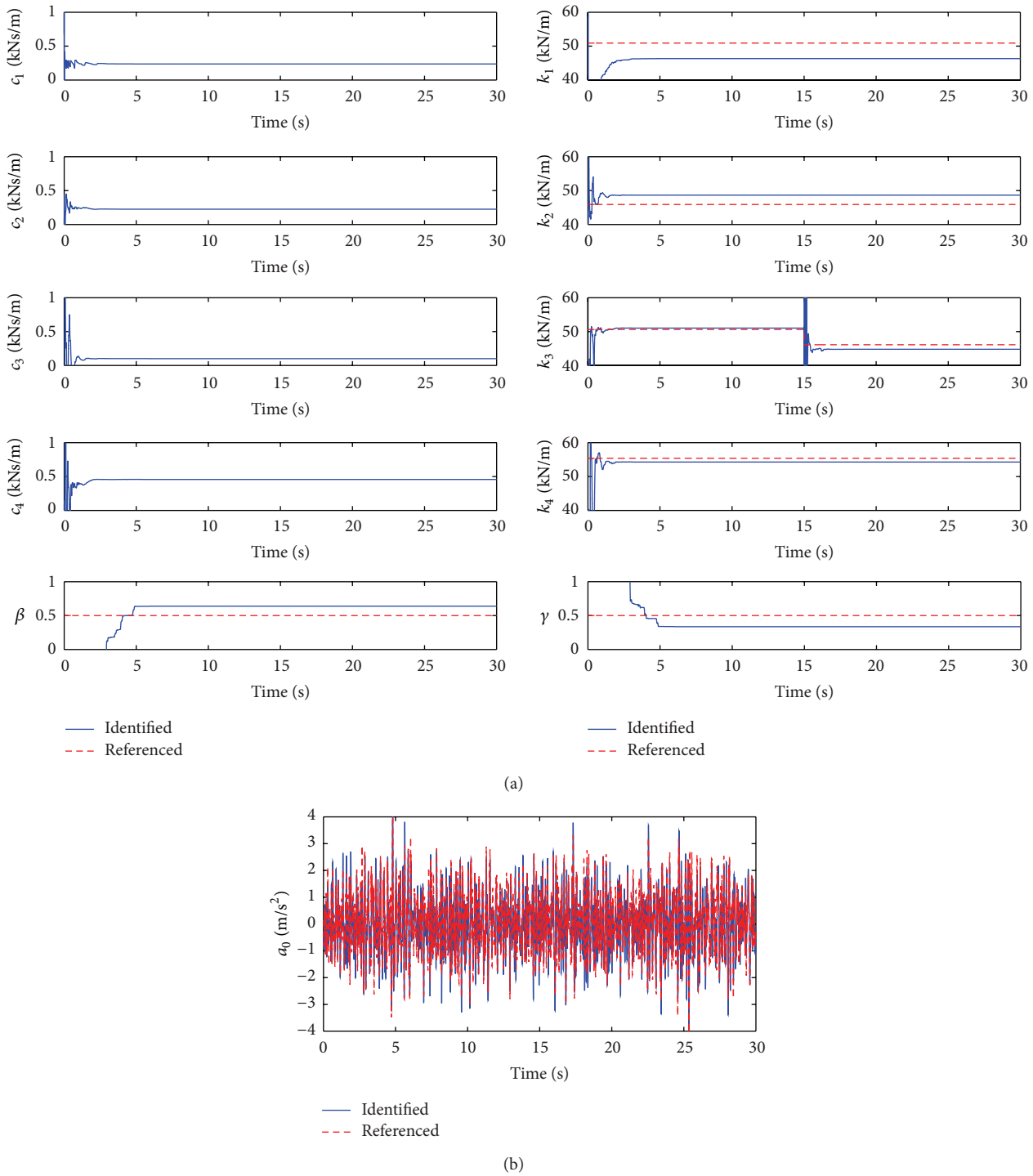

Figure 8: Identified results for Case 2: (a) identified parameters; (b) identified excitation.

of a small amplitude vibration compared to the four cases investigated. The capability and accuracy of the Bouc-Wen model for describing the behavior of the base-isolation layer are demonstrated by comparisons of the measured data to the model identification results, shown in Figure 4(b) as solid curves. It is seen that the results coincide well with the measured loops denoted by the dashed curves [40]. In these tests, two stiffness element devices, each one consisting of a hydraulic cylinder-piston and a bracing system, are installed in the second and third story unit separately as shown in

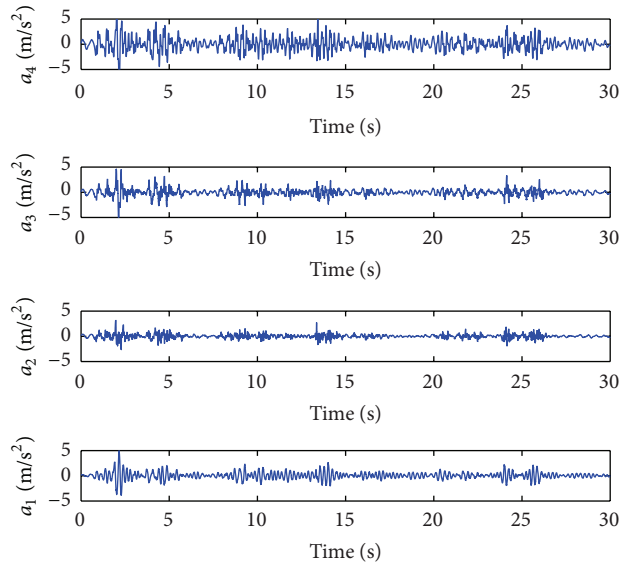

FIGURE 9: Measured acceleration responses for Case 3.

Figure 1. From the experimental data of the HCP, a gas pressure at $P_0 = 0.45$ MPa results in an effective stiffness of 4.5 kN/m for SED; that is, $K_{hi} = K_{ei} = 4.5$ kN/m and a gas pressure at $P_0 = 0.75$ MPa results in an effective stiffness of 7.5 kN/m for SED; that is, $K_{hi} = K_{ei} = 7.5$ kN/m. These values of effective stiffness will be used for the different damage severities. The results for the four typical cases are presented in what follows.

4.1. Case 1: Single Damage in Second Story (White Noise Excitation). In this test, a band-limited white noise excitation in the frequency range of 1–25 Hz with PGA of 0.32 g is used and single damage in second story is simulated. The HCP in second story is filled with air at a pressure of 0.75 MPa, so that the effective stiffness of the corresponding SED is 7.5 kN/m. Thus, the stiffness of the second story is $k_2 = 45.9$ kN/m + 7.5 kN/m = 53.4 kN/m, whereas the stiffness of other three stories is $k_1 = 50.9$ kN/m, $k_3 = 46.1$ kN/m, and $k_4 = 55.4$ kN/m. During the test, both valves of the HCP are closed at the beginning and are opened simultaneously at $t = 15$ s, so that the stiffness of the second story reduces abruptly from 53.4 kN/m to 45.9 kN/m at $t = 15$ s. The acceleration responses of all stories, a_1, a_2, a_3, and a_4, are measured and presented in Figure 5.

Based on the acceleration responses shown in Figure 5, the equation of motion for analytical base-isolated building model in (20) and the ASNLSE-UI approach, the unknown parameters, including the stiffness and damping of all stories, that is, k_i and c_i ($i = 1, 2, 3, 4$), and the hysteretic information of the first story (base-isolation layer), of which the nonlinear hysteretic characteristic is described by the Bouc-Wen model, that is, β and γ, as well as the unknown load $\ddot{x}_0$, can be identified by using the recursive solution, (5)–(9) and (11)–(16). For the ASNLSE-UI recursive solution described previously, the following initial values are assumed: (i) the initial values for k_i and c_i are $k_{i0} = 40$ kN/m and $c_{i0} = 0.1$ kNs/m ($i = 1, 2, 3, 4$); (ii) the initial values for β and γ are $\beta = 0.1$ and $\gamma = 0.1$; (iii) the initial values for the displacements and velocities are zero; that is, $\mathbf{x} = \mathbf{0}$, $\dot{\mathbf{x}} = \mathbf{0}$; (iv) the initial matrixes for $\mathbf{P}_0$ and $\mathbf{P}_{0|0}$ are $\mathbf{P}_0 = 10^5\mathbf{I}_{10}$, $\mathbf{P}_{0|0} = \mathbf{I}_8$, respectively, where $\mathbf{I}_j$ is a $(j \times j)$ unit matrix. In all the experimental studies to be presented later, the same initial values will be used.

Based on the ASNLSE-UI recursive solution along with analytical model for base-isolated building and the measured data shown in Figure 5, the identified quantities are presented in Figure 6 denoted by solid curves. The dashed curves represent the reference parameters obtained by FEM for the stiffness and experiments for the hysteretic parameters in Figure 6(a), and the measured base acceleration in Figure 6(b). In Figure 6, the solid curves almost coincide with the dashed curves, indicating that the accuracy of the ASNLSE-UI approach is good. The difference between the solid and dashed curves is expected due to the structural uncertainty of the test model, including the shear-beam assumption. Figure 6(a) clearly demonstrates that the ASNLSE-UI approach is capable of tracking the variation of stiffness parameters, leading to the detection of structural damages. Likewise, the ASNLSE-UI predictions for the unknown excitation are also good.

4.2. Case 2: Single Damage in Third Story (White Noise Excitation). In this test, a band-limited white noise excitation in the frequency range of 1.9–25 Hz with PGA of 0.44 g is used and single damage in third story is simulated. The HCP in third story is filled with air at a pressure of 0.45 MPa, so that the effective stiffness of the corresponding SED is 4.5 kN/m. Thus, the stiffness of the third story is $k_3 = 46.1$ kN/m + 4.5 kN/m = 50.6 kN/m, whereas the stiffness of other three stories is $k_1 = 50.9$ kN/m, $k_2 = 45.9$ kN/m and $k_4 = 55.4$ kN/m. During the test, both valves of the HCP are closed at the beginning and are opened simultaneously at $t = 15$ s, so that the stiffness of the third story reduces abruptly from 50.6 kN/m to 46.1 kN/m at $t = 15$ s. The acceleration responses of all stories, a_1, a_2, a_3 and a_4, are measured and presented in Figure 7.

Similarly, based on the experimental data shown in Figure 7 and the ASNLSE-UI approach, the unknown quantities are identified. The identified quantities and the reference ones are presented in Figure 8. It is seen that they agree well each other. In Case 2, the place and the severity of single damage are different from that in Case 1. The intensity of the white noise excitation in Case 2 is far greater than that in Case 1, so the level of experimental noise is much higher than that in Case 1. Besides, the strong excitation may lead to some unexpected slight swing in the test due to the character of the base-isolated building model. The swing also introduces some noise into the system. Consequently, the differences between identified results and referenced ones in Case 2 are a little larger than that in Case 1 but the results are acceptable. Based on the results of Case 1 and Case 2, it may be concluded that the ASNLSE-UI predictions are quite reasonable.

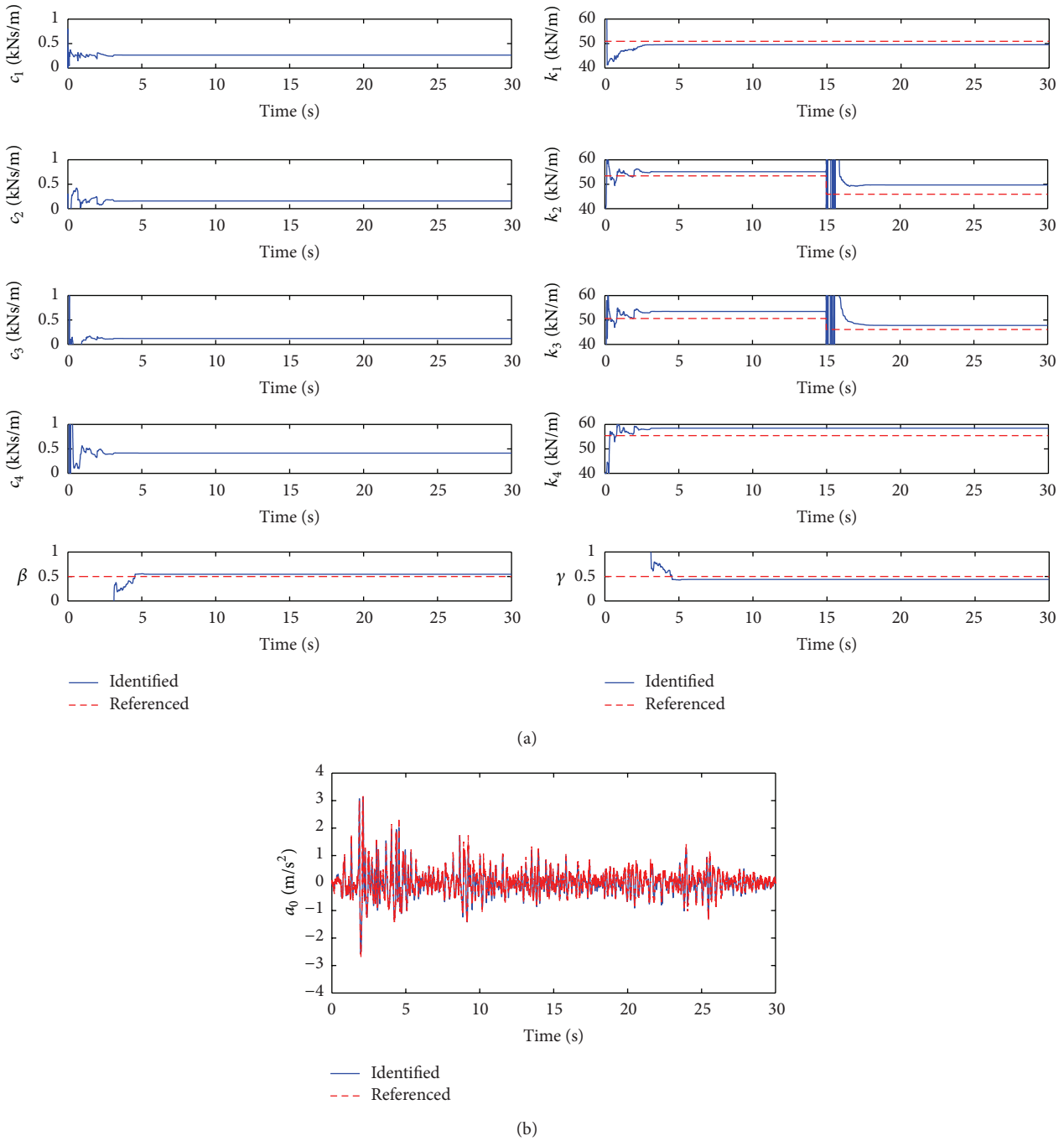

Figure 10: Identified results for Case 3: (a) identified parameters; (b) identified excitation.

4.3. Case 3: Damages in Second and Third Stories (El Centro Earthquake Excitation). In this test, El Centro earthquake excitation, of which the energy distribution is uniform, is used and damages in second and third story are simulated. Due to the limitation of the shake table, a high-pass filtering process is conducted, resulting in the fact that the actual excitation in the frequency range of 1.5–5 Hz with PGA of 0.32 g is slightly different but very close to the original El Centro earthquake signal. The filtered El Centro earthquake excitation is actually used as the unknown input to the test. The HCPs in second and third stories are filled with air at a pressure of 0.75 MPa and 0.45 MPa, respectively, so that the effective stiffness of the corresponding SEDs is 7.5 kN/m and 4.5 kN/m. Thus, the stiffness of the second and third stories is $k_2 = 45.9\,\text{kN/m} + 7.5\,\text{kN/m} = 53.4\,\text{kN/m}$ and $k_3 = 46.1\,\text{kN/m} + 4.5\,\text{kN/m} = 50.6\,\text{kN/m}$, whereas the stiffness of the other two stories is $k_1 = 50.9\,\text{kN/m}$ and $k_4 = 55.4\,\text{kN/m}$. During the test, the valves of the two HCPs are closed at the beginning and are opened simultaneously at $t = 15\,\text{s}$, so that the stiffness of the second story reduces abruptly from

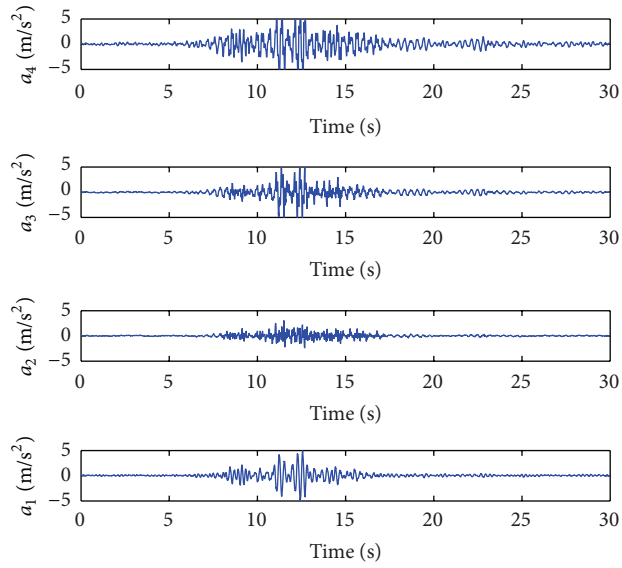

Figure 11: Measured acceleration responses for Case 4.

53.4 kN/m to 45.9 kN/m at $t = 15$ s and the stiffness of the third story reduces abruptly from 50.6 kN/m to 46.1 kN/m at the same time. The acceleration responses of all stories, a_1, a_2, a_3, and a_4, are measured and presented in Figure 9.

Similarly, based on the experimental data shown in Figure 9 and the ASNLSE-UI approach, the unknown quantities are identified. The identified quantities and the reference ones are shown in Figure 10. It is seen that they agree well with each other. In Case 3, two damages occur at the same time in different places with different severities. The identified results illustrate that the adaptive technique is able to track the multi-time-varying parameters effectively without influence on other constant parameters and is less sensitive to noise. It is observed form Figure 10 that the ASNLSE-UI predictions are effective even under the earthquake excitation for the complex multidamage tracking.

4.4. Case 4: Damages in Second and Third Stories (Kobe Earthquake Excitation). In this test, Kobe earthquake excitation, of which the energy distribution is high in short time, is used and damages in second and third story are simulated. Due to the limitation of the shake table, a high-pass filtering process is conducted. The filtered Kobe earthquake excitation in the frequency range of 1.8–3 Hz with PGA of 0.28 g, which retains the original characteristics of Kobe earthquake signal, is actually used as the unknown input to the test. The HCPs and SEDs configurations are similar to that of Case 3, so the stiffness conditions of each story are the same as the ones in Case 3. The most intensive portion of Kobe earthquake occurs prior to 12 s and damage may occur immediately after 12 s. Hence, one damage is simulated in third story at $t = 12$ s, and the other is simulated in second story at $t = 20$ s to approximate the real situation. During the test, the valves of the two HCPs are closed at the beginning. Then the valves of the HCP in third story are opened at $t = 12$ s, and the valves of the HCP in second story are open at $t = 20$ s, so that the stiffness of the third story reduces abruptly from 50.6 kN/m to 46.1 kN/m at $t = 12$ s and the stiffness of the second story reduces abruptly from 53.4 kN/m to 45.9 kN/m at $t = 20$ s. The acceleration responses of all stories, a_1, a_2, a_3, and a_4, are measured and presented in Figure 11.

Based on the experimental data shown in Figure 11 and the ASNLSE-UI approach, the unknown quantities are identified. The identified quantities and the reference ones are presented in Figure 12. It is seen that they agree well each other. In Case 4, the place and the severity of the damages approximate the real situation that a base-isolated building suffers from Kobe earthquake excitation. Again, Figure 12 demonstrates that the ASNLSE-UI predictions are quite reasonable, and the trend of predictions is consistent with that of all other three cases.

The theoretical and experimental studies show that the test results are consistent and reasonable for the four typical cases. The discrepancies between the identified results and the referenced ones may be due to the structural uncertainties of the test model, the Boun-Wen model simplification for reducing computational effort, and the uncertainty of the shear-beam model used in the ASNLSE-UI analysis. In particular, the masses of columns are not distributed to the stories in the analysis model. Besides, the convergence of the solutions should be faster when higher sampling frequency is used due to the use of Newmark-β method. Consequently, more accurate models, higher sampling frequency, and lower noises would have reduced the discrepancies between the identified results and the true values and thus eliminated damage misjudgments. It should be mentioned that the discrepancies are acceptable in practical applications, as can be seen from Table 1, and the improved ASNLSE-UI approach is capable of tracking the damages of base-isolated building.

5. Conclusion

In this research, the recently proposed approach, the adaptive sequential nonlinear least square estimation with unknown inputs, has been developed along with Bouc-Wen model representing the nonlinear hysteretic behavior and species-based quantum-behaved particle swarm optimization achieving the adaptive tracking for the health monitoring of nonlinear hysteretic system. Experimental studies have been performed to verify the capability of the proposed approach in real-time tracking the structural damage and simultaneously identifying the unknown input. A series of experiments have been performed on a scaled 3-story base-isolated building model. To simulate the structural damage during the test, an innovative stiffness element device has been proposed to reduce the stiffness of some building stories. Different damage scenarios under different loading conditions, including white noise excitations and typical earthquake excitations, have been simulated and tested. Measured acceleration response data and the ASNLSE-UI approach have been used to track the variation of the parameters in different stories as well as to identify the unknown load during the test. The identified results correlate reasonably well with the reference

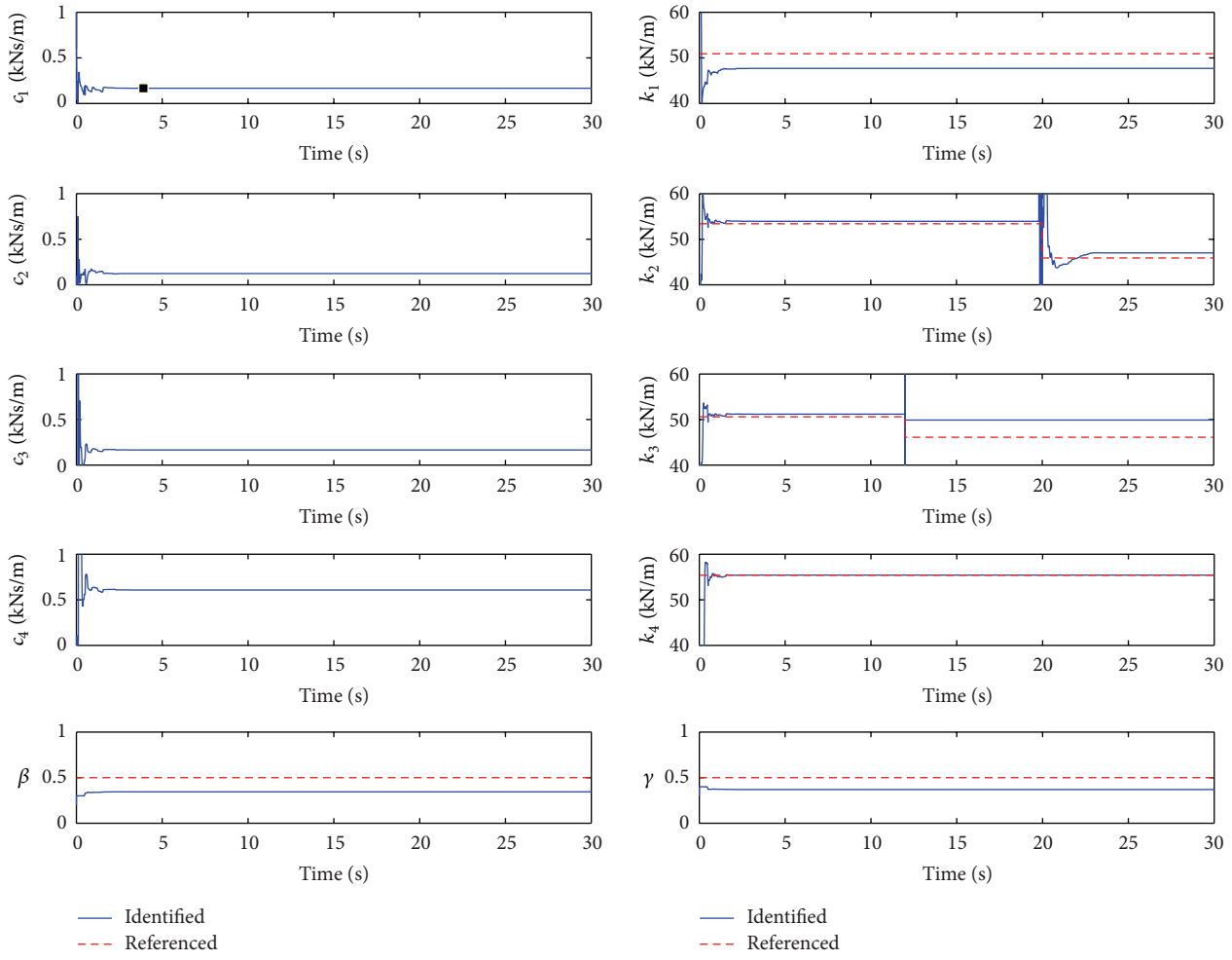

(a)

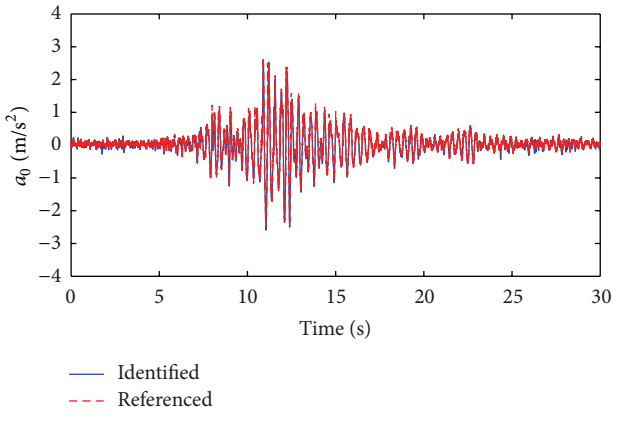

(b)

FIGURE 12: Identified results for Case 4: (a) identified parameters; (b) Identified excitation.

ones. Experimental studies demonstrate that the ASNLSE-UI approach is capable of real-time tracking the damages of base-isolated building and simultaneously identifying the unknown inputs.

Conflict of Interests

The authors declare that there is no conflict of interests regarding the publication of this paper.

Table 1: Identified results for all cases.

Case	Parameter	c_1	c_2	c_3	c_4	k_1	k_2	k_3	k_4	β	γ
	Ref. values	—	—	—	—	50.9	53.4 → 45.9	50.6 → 46.1	55.4	0.5	0.5
Case 1	Identified	0.37	0.14	0.13	0.42	47.79	55.16 → 46.82	47.85	56.87	0.57	0.44
	Deviation (%)	—	—	—	—	6.11	3.30, 2.00	3.80	2.65	13.20	11.40
Case 2	Identified	0.24	0.23	0.10	0.46	46.32	48.65	51.03 → 44.78	54.28	0.64	0.34
	Deviation (%)	—	—	—	—	9.00	5.99	0.85, 2.86	2.02	27.80	32.80
Case 3	Identified	0.26	0.16	0.12	0.41	49.53	55.11 → 49.70	53.49 → 47.77	58.44	0.55	0.44
	Deviation (%)	—	—	—	—	2.69	3.20, 8.28	5.71, 3.62	5.49	9.00	12.00
Case 4	Identified	0.17	0.12	0.17	0.61	47.69	53.94 → 46.99	51.17 → 49.88	55.41	0.35	0.37
	Deviation (%)	—	—	—	—	6.31	1.00, 2.37	1.13, 8.20	0.02	31.00	26.20

c_i unit: kNs/m; k_i unit: kN/m ($i = 1, 2, 3, 4$).

Acknowledgments

This research is partially supported by the National Natural Science Foundation of China (Grant no. 11172128), the US National Science Foundation (no. CMMI-0853395), the Funds for International Cooperation and Exchange of the National Natural Science Foundation of China (Grant no. 61161120323), the Specialized Research Fund for the Doctoral Program of Higher Education of China (Grant no. 20123218110001), the Jiangsu Foundation for Excellent Talent of China (Grant no. 2010-JZ-004), the Jiangsu Graduate Training Innovation Project (CXLX11_0171), and the Priority Academic Program Development of Jiangsu Higher Education Institutions.

References

[1] D. Bernal and J. Beck, "Special section: phase I of the IASC-ASCE structural health monitoring benchmark," *Journal of Engineering Mechanics*, vol. 130, no. 1, pp. 1–127, 2004.

[2] F. K. Chang, "Structural health monitoring," in *Proceeding of 8th International Workshop*, Stanford, Calif, USA, 2011.

[3] R. Bighamian and H. R. Mirdamadi, "Input/output system identification of simultaneous mass/stiffness damage assessment using discrete-time pulse responses, differential evolution algorithm, and equivalent virtual damped SDOF," *Structural Control and Health Monitoring*, vol. 24, no. 4, pp. 576–592, 2012.

[4] J. Humar, A. Bagchi, and H. Xu, "Performance of vibration-based techniques for the identification of structural damage," *Structural Health Monitoring*, vol. 5, no. 3, pp. 215–241, 2006.

[5] Y. S. Lee, S. Tsakirtzis, A. F. Vakakis, L. A. Bergman, and D. M. McFarland, "A time-domain nonlinear system identification method based on multiscale dynamic partitions," *Meccanica*, vol. 46, no. 4, pp. 625–649, 2011.

[6] J.-W. Lin, R. Betti, A. W. Smyth, and R. W. Longman, "On-line identification of non-linear hysteretic structural systems using a variable trace approach," *Earthquake Engineering and Structural Dynamics*, vol. 30, no. 9, pp. 1279–1303, 2001.

[7] J. N. Yang and S. Lin, "Identification of parametric variations of structures based on least squares estimation and adaptive tracking technique," *Journal of Engineering Mechanics*, vol. 131, no. 3, pp. 290–298, 2005.

[8] O. Maruyama and M. Hoshiya, "System identification of an experimental model by extended kalman filter," in *Proceedings of Structural Safety and Reliability (ICOSSAR '01)*, 2001.

[9] J. N. Yang, S. Lin, H. Huang, and L. Zhou, "An adaptive extended Kalman filter for structural damage identification," *Structural Control and Health Monitoring*, vol. 13, no. 4, pp. 849–867, 2006.

[10] W. Meiliang and A. W. Smyth, "Application of the unscented Kalman filter for real-time nonlinear structural system identification," *Structural Control and Health Monitoring*, vol. 14, no. 7, pp. 971–990, 2007.

[11] J. N. Yang, H. Huang, and S. Lin, "Sequential non-linear least-square estimation for damage identification of structures," *International Journal of Non-Linear Mechanics*, vol. 41, no. 1, pp. 124–140, 2006.

[12] T. Sato and K. Qi, "Adaptive H_∞ filter: its application to structural identification," *Journal of Engineering Mechanics*, vol. 124, no. 11, pp. 1233–1240, 1998.

[13] T. Sato and M. Chung, "Structural identification using adaptive Monte Carlo filter," *Journal of Structural Engineering*, vol. 51, pp. 471–477, 2005.

[14] D. Wang and A. Haldar, "System identification with limited observations and without input," *Journal of Engineering Mechanics*, vol. 123, no. 5, pp. 504–510, 1997.

[15] C. D. Johnson, "Identification of unknown, time-varying forces/moments in dynamics and vibration problems using a new approach to deconvolution," *Shock and Vibration*, vol. 5, no. 3, pp. 181–197, 1998.

[16] G. P. Cimellaro, S. Piantà, and A. De Stefano, "Output-only modal identification of ancient L' aquila city hall and civic tower," *Journal of Structural Engineering*, vol. 138, no. 4, pp. 481–491, 2012.

[17] Y. G. Qu, H. X. Hua, and G. Meng, "A domain decomposition approach for vibration analysis of isotropic and composite cylindrical shells with arbitrary boundaries," *Composite Structures*, vol. 95, pp. 307–321, 2013.

[18] J. Lardiès, "A stochastic realisation algorithm with application to modal parameter estimation," *Mechanical Systems and Signal Processing*, vol. 15, no. 2, pp. 275–285, 2001.

[19] S. R. Ibrahim, "Efficient random decrement computation for identification of ambient responses," in *International Society for Optical Engineering*, vol. 4359 of *Proceedings of SPIE*, pp. 1–6, Kissimmee, Fla, USA, 2001.

[20] F. Kozin, "Estimation of parameters for system driven by white noise excitation," in *Proceedings of the IUTAM Symposium on Random Vibrations and Reliability*, pp. 163–173, Frankfurt Ioder, Germany, 1985.

[21] K. Toki, T. Sato, and J. Kiyono, "Identification of structural parameter s and input ground motion from response time history," *Structural Engineering*, vol. 6, no. 2, pp. 413–421, 1989.

[22] X. Ling and A. Haldar, "Element level system identification with unknown input with Rayleigh damping," *Journal of Engineering Mechanics*, vol. 130, no. 8, pp. 877–885, 2004.

[23] J. Chen and J. Li, "Simultaneous identification of structural parameters and input time history from output-only measurements," *Computational Mechanics*, vol. 33, no. 5, pp. 365–374, 2004.

[24] J.-Y. Wang, J.-Y. Chen, Z.-K. Li, and J.-Y. Liu, "Study on identification method for a structure with non-proportional damping and unknown input," *Journal of Vibration and Shock*, vol. 26, no. 4, pp. 119–125, 2007.

[25] S. S. Law, K. Zhang, and Z. D. Duan, "Structural damage detection from coupling forces between substructures under support excitation," *Engineering Structures*, vol. 32, no. 8, pp. 2221–2228, 2010.

[26] J. N. Yang, S. Pan, and S. Lin, "Least-squares estimation with unknown excitations for damage identification of structures," *Journal of Engineering Mechanics*, vol. 133, no. 1, pp. 12–21, 2007.

[27] J. N. Yang, S. Pan, and H. Huang, "An adaptive extended Kalman filter for structural damage identifications II: unknown inputs," *Structural Control and Health Monitoring*, vol. 14, no. 3, pp. 497–521, 2007.

[28] J. N. Yang and H. Huang, "Sequential non-linear least-square estimation for damage identification of structures with unknown inputs and unknown outputs," *International Journal of Non-Linear Mechanics*, vol. 42, no. 5, pp. 789–801, 2007.

[29] J. N. Yang and H. Huang, "Damage tracking of base-isolated building using sequential nonlinear LSE with unknown inputs and outputs," in *Smart Structures and Materials: Sensors and Smart Structures Technologies for Civil, Mechanical, and Aerospace Systems*, Proceedings of SPIE, San Diego, Calif, USA, March 2006.

[30] S. Narasimhan, S. Nagarajaiah, E. A. Johnson, and H. P. Gavin, "Smart base-isolated benchmark building. Part I: problem definition," *Structural Control and Health Monitoring*, vol. 13, no. 2-3, pp. 573–588, 2006.

[31] B.-J. Chen, C. S. Tsai, L. L. Chung, and T.-C. Chiang, "Seismic behavior of structures isolated with a hybrid system of rubber bearings," *Structural Engineering and Mechanics*, vol. 22, no. 6, pp. 761–783, 2006.

[32] J. Zhao, J. Sun, C.-H. Lai, and W. Xu, "An improved quantum-behaved particle swarm optimization for multi-peak optimization problems," *International Journal of Computer Mathematics*, vol. 88, no. 3, pp. 517–532, 2011.

[33] L. Zhou, S. Wu, and J. N. Yang, "Experimental study of an adaptive extended Kalman filter for structural damage identification," *Journal of Infrastructure Systems*, vol. 14, no. 1, pp. 42–51, 2008.

[34] Q. Yin and L. Zhou, "Structural damage identification based on GA optimized least square estimation," *Journal of Vibration and Shock*, vol. 29, no. 8, pp. 155–159, 2010.

[35] J. N. Yang, J.-H. Kim, and A. K. Agrawal, "Resetting semiactive stiffness damper for seismic response control," *Journal of Structural Engineering*, vol. 126, no. 12, pp. 1427–1433, 2000.

[36] Y. K. Wen, "Methods of random vibration for inelastic structures," *Applied Mechanical Reviews*, vol. 42, no. 2, pp. 39–52, 1989.

[37] Y. K. Wen and A. H. Ang, "Inelastic modeling and system identification," in *Structural Safety Evaluation Based on System Identification Approaches*, pp. 142–160, 1988.

[38] F. Ma, H. Zhang, A. Bockstedte, G. C. Foliente, and P. Paevere, "Parameter analysis of the differential model of hysteresis," in *Proceedings of the IUTAM Symposium on Nonlinear Stochastic Dynamics*, pp. 257–268, Springer, 2003.

[39] X.-M. Wang and L. Zhou, "Modeling of a rubber bearing and its parameters estimation based on its dynamic response," *Journal of Vibration and Shock*, vol. 27, no. 1, pp. 146–150, 2008.

[40] Q. Yin, L. Zhou, and X. Wang, "Parameter identification of hysteretic model of rubber-bearing based on sequential nonlinear least-square estimation," *Earthquake Engineering and Engineering Vibration*, vol. 9, no. 3, pp. 375–383, 2010.

[41] A. Agrawal, P. Tan, S. Nagarajaiah, and J. Zhang, "Benchmark structural control problem for a seismically excited highway bridge. Part I: phase I problem definition," *Structural Control and Health Monitoring*, vol. 16, no. 5, pp. 509–529, 2009.